Parallax Compensation in Offset-Mounted Spherical Near-Field Vehicular Antenna Measurements With Probe Effects for FFT-Based NFFFTs

Cosme Culotta-López, *Member, AMTA*
Gil Yemini, *Member, AMTA*
Grigory Kuznetsov, *Member, AMTA*
Orbit/FR Engineering Ltd. (MVG), Israel
cosme.culottalopez@mvg-world.com

Francesco Saccardi, *Fellow, AMTA*
Andrea Giacomini, *Senior Member, AMTA*
Lars J. Foged, *Fellow, AMTA*
Microwave Vision Italy SRL (MVG), Italy
francesco.saccardi@mvg-world.com

Nicolas Gross
Stéphane Issartel
Microwave Vision Group (MVG), France
nicolas.gross@mvg-world.com

***Abstract*—Spherical Near-Field antenna measurements are broadly used for vehicular measurements, which almost always include several antennas. Due to the large size of vehicles and the reduced size of near-field ranges, it is often impossible to displace the vehicle so that the desired Antenna Under Test (AUT) be in the center of the measurement sphere - and when it is possible, it is highly impractical to repeatably displace the vehicle for each of the antennas. Nevertheless, it is often required to retrieve the radiation characteristics of the AUT as if it were centered. In this work, Parallax-based methods for the correction of near-field acquired data are discussed, and a novel method based on the correction of the probe's relative view angle and distance to the offset AUT is introduced. This method, additionally, does not require any matrix (pseudo)inversion for the calculation of the Spherical Wave Coefficients (SWCs) and can be solved with classical FFT-based Near-Field-to-Far-Field Transformations (NFFFT) based on the Wacker transmission formula.**

I. Introduction

Modern vehicles are characterized by the integration of multiple communication systems, strategically positioned within it. For practical reasons, Spherical Near-Field (SNF) measurements are frequently conducted with the Device Under Test (DUT) centrally located within the measurement system. However, due to the dimensions and geometry of vehicles, the DUT may be offset from the center of the measurement system, especially at high frequencies, where the equivalent electrical size can be very large. Additionally, the Antenna Under Test (AUT) may also be offset from the center of the DUT, further complicating the geometry of the problem. Direct measurements in such a configuration can introduce distortions in the measured pattern, particularly when the measurement distance is reduced. These distortions can be mitigated if the AUT's position is accurately known. Compensation can be applied by accounting for the difference in Free Space Path Losses (FSPL compensation) at each probe position, and by also considering the variation in view angles at each probe position (Parallax compensation) [1]–[3]. This involves adding both a magnitude and a phase offset to each measurement point, both in the single and in the multi-probe case. However, and considering a measurement in the Near Field (NF), probe effects also play a role which, precisely because of the NF nature of the problem, varies with both the view angle and the distance between the probe and the AUT.

In this paper, offset Spherical Near-Field (SNF) measurements are compensated calculating the mentioned magnitude and phase offsets as FSPL and Parallax compensations and, additionally, the probe effects are calculated and compensated as an additional magnitude/phase offset.

To achieve this, the known Spherical Wave Coefficients (SWCs) of the probe are inserted into the Spherical Wave Expansion (SWE) to retrieve the probe pattern at the distance of each measurement point to the AUT. At the same time, the probe pattern is calculated at the distance between the probe and the center of the measurement system. This is the "reference point". Then, the differences in magnitude and phase between the pattern of the probe at the relative observation point and the reference point is computed, and added to the magnitude and phase offsets obtained through the FSPL and Parallax compensations.

By applying this technique, it is possible to treat the measurement as if it had been measured at the center of the measurement system, thus, treating the local minimum sphere around the AUT as if it were centered at the center of the measurement system. Additionally and for most commercially available systems using equiangular sampling, this means that, after the introduced compensation is applied,

classical FFT-based Near-Field-to-Far-Field Transformations (NFFFTs), based on the Wacker algorithm, can be used, thus avoiding the long computation times and numerical instability of other methods, such as pseudoinverse-based matricial methods.

II. Theoretical Overview

This section delves into the Spherical Wave Expansion (SWE). It is used to describe the electromagnetic fields on a spherical surface encompassing a radiating entity. This methodology is foundational in Spherical Near-Field (SNF) antenna assessments [4]. As illustrated in [5], [6], SWE can be formulated as a linear equation system $\boldsymbol{y} = \mathbf{A}\boldsymbol{x}$, where the performance of the matrix $\mathbf{A}$ is influenced by the sampling pattern and the solution of the system depends on the invertibility of $\mathbf{A}$.

A. The Transmission Formula

The generalized probe-corrected transmission expression [4] is given by:

$$\begin{aligned} &w(A,\chi,\theta,\phi) = \\ &= \sum_{s=1}^{2} \sum_{\mu=-\nu_{\max}}^{\mu=\nu_{\max}} \sum_{n=1}^{\infty} \sum_{m=-n}^{n} T_{smn} D^{n}_{\mu m}(\theta,\phi,\chi) P_{s\mu n}(kA), \end{aligned} \tag{1}$$

where $w(A,\chi,\theta,\phi)$ represents the signal measurement at distance A, polarization angle χ, and rotation angles θ and ϕ. Here, T_{snm} are the transmission coefficients, or Spherical Wave Coefficients (SWCs) of the measured Antenna Under Test (AUT), $D^{n}_{\mu m}(\theta,\phi,\chi) = e^{jm\phi} d^{n}_{\mu m}(\theta) e^{j\mu\chi}$ signifies the Euler rotation of spherical waves, known as Wigner D-functions, and $P_{s\mu n}(kA)$ is the probe response constant. The probe response constant $P_{s\mu n}(kA)$ consists of the SWCs of the probe in receive mode $R_{\sigma\mu\nu}$ multiplied by the translation constants $C^{sm}_{\sigma\mu\mu}(kA)$, so that:

$$P_{s\mu n} = \sum_{\sigma\nu} C^{sm}_{\sigma\mu\nu}(kA) R_{\sigma\mu\nu}, \tag{2}$$

with the Greek subindices being the probe counterpart of the Latin smn subindices, corresponding to the AUT. The translation constants $C^{sm}_{\sigma\mu\mu}(kA)$ take the SWCs of the probe $T_{\sigma\mu\nu}$, centered in the coordinate system of the measurement, i.e., where the AUT is centered, and displace them along the $z-$axis to the measurement distance A. Expressing them in receive mode, i.e., converting them from $T_{\sigma\mu\nu}$ to $R_{\sigma\mu\nu}$, the measurement configuration is simulated analytically. In the literature, Eq. (1) is known as the Jensen-Wacker transmission formula [4].

Given that antennas are band-limited, the summation over n can be truncated to a band-limit constant B, so that $1 \leq n \leq B$. This constraint also makes the summation over m, $-n \leq m \leq n$, finite. This upper band limit is defined as:

$$B = kr_0 + B_0, \tag{3}$$

where k is the wavenumber, r_0 is the radius of the smallest sphere enclosing the Antenna Under Test (AUT), and B_0 is a stability and accuracy constant, often taken as $B_0 = 10$. Higher-order modes do exist but are significantly attenuated, limiting their contribution to the far-field radiation pattern. Additionally, s is restricted to $s = 1$ and $s = 2$, corresponding to TE and TM modes propagation, respectively. Given these conditions, the total number of modes N is calculated by:

$$N = 2B(B+2) = 2B^2 + 4B. \tag{4}$$

The generalized probe-corrected transmission formula can be expressed as a matrix equation:

$$\boldsymbol{w} = \boldsymbol{\Psi}\boldsymbol{q}, \tag{5}$$

where $\boldsymbol{w} \in \mathbb{C}^M$ is the measurement signal vector, $\boldsymbol{\Psi} \in \mathbb{C}^{M\times N}$ is the matrix containing samples of Euler rotation, or Wigner D-functions, and probe response constants, and $\boldsymbol{q} \in \mathbb{C}^N$ is the antenna transmission coefficients vector. For this system, considering the previous points, $M = N$ measurements are sufficient to resolve the linear system. However, typical equiangular sampling results in:

$$\begin{aligned} M = M_\chi M_\theta M_\phi &= 2(B+1)(2B+1) = \\ &= 4B^2 + 6B + 2 > 2N, \end{aligned} \tag{6}$$

which is nearly double the necessary samples. Many equiangular sampling points are linearly dependent, contributing to the inefficiency of this approach, although it provides a well-conditioned problem [5] and, due to the vectorially equidistant nature of this sampling, it can be solved by application of FFT-based Near-Fied-to-Far-Field Transformations (NFFFTs), based on the Wacker algorithm [4], [7].

While the alternative of solving Eq. (5) by calculating the (pseudo)inverse of $\boldsymbol{\Psi} \in \mathbb{C}^{M\times N}$ does allow for a non-regular sampling and is theoretically feasible, it is not without potential pitfalls. The invertibility of a matrix is contingent upon certain conditions, such as non-singularity and numerical stability, which may not always be guaranteed in practical applications. In cases where the matrix is ill-conditioned or nearly singular, inversion can lead to significant numerical inaccuracies, thereby compromising the reliability of the solution. Therefore, alternative approaches that do not rely solely on matrix inversion may be preferable, especially in scenarios where the stability and robustness of the solution are paramount.

B. Equiangular Sampling and Offset Measurements

The purpose of equiangular sampling is to produce a set of equally spaced points, which is necessary for applying the Wacker algorithm as the solver. Additionally, this approach ensures sufficient data collection to prevent aliasing by adhering to the Whittaker-Nyquist-Kotelnikov-Shannon sampling theorem, commonly referred to as the Nyquist-Shannon theorem or simply the Nyquist theorem in the context of antenna measurements [8], [9].

Following Eq. (3), the band-limit constant B depends on the radius of the minimum sphere enclosing the AUT, r_0. For an offset measurement in which the AUT is displaced to position $\vec{a} = (x_0, y_0, z_0)$ with $|\vec{a}| > 0$, the radius of the new minimum sphere enclosing the AUT reads $r_1 = r_0 + |\vec{a}| > r_0$ and, thus, $B' > B$ and the new number of samples for equiangular sampling defined by Eq. (6) increases, so that $M' > M$. The Jensen-Wacker transmission formula in Eq. (1) can be rewritten for the case of an offset $\vec{a} = (x_0, y_0, z_0)$ corresponding to a displacement of magnitude $|\vec{a}|$ in the (θ_a, ϕ_a) direction by using the translation coefficients of spherical waves, as well as their rotation operators, so that:

$$\begin{aligned} T'_{smn} &= \sum_{\substack{hkl \\ m}} C^{sm}_{hkl}(k|\vec{a}|) T_{hkl} D^{l}_{mk}(\theta_a, \phi_a) = \\ &= \sum_{\substack{hkl \\ m}} C^{sm}_{hkl}(k|\vec{a}|) T_{hkl} e^{jk\phi_a} d^{n}_{mk}(\theta_a). \end{aligned} \tag{7}$$

The new displaced SWCs of the AUT described in Eq. (7) is then inserted into the Jensen-Wacker formula of Eq. (1) replacing the centered SWCs T_{smn}, which correspond to T_{hkl} in Eq. (7).

Additionally, in case the offset is due to the AUT being attached to an additional, large reflective structure that cannot be placed so that the AUT is in the center of the measurement, the results will suffer from reflections. The structure will be within the measurement sphere, and the SWCs corresponding to the reflections with it will be mixed with the AUT's with no filtering occurring [10], [11] unless advanced reflection suppression techniques can be used, such as MARS [12], which indeed require the acquisition of the higher number of samples $M' > M$. Alternatively, the original number of samples M can be used to process offset measurements and suppress echo with the Translated-SWE (TSWE) [13], [14] method. This method relies on the projection of the sampling points on the displaced minimum sphere, centered in the AUT and enclosing it, onto the larger measurement sphere resulting from the offset, centered at the center of the measurement sphere. Therefore, the number of measurement points does not increase due to the offset, but the equidistant property of the sampling in angular terms gets lost due to the projection if the offset is along the $x-$ and/or $y-$axes [13]. Due to this, FFT-based NFFFTs cannot be used and matrix inversion problems arise instead, which introduce computational complexity.

III. Parallax Compensation

The differences introduced by an offset of the AUT in the measurement as described by Eq. (7) are the additional translation constants and rotation of spherical waves, which enlarge the minimum sphere radius by $|\vec{a}|$ and, thus, force the acquisition of additional measurement points as given by Eqs. (6) and (3) and potentially introduce the effect of further radiating and reflecting elements into the minimum sphere. Ideally, if the measurement sphere, with radius A, is larger than the minimum sphere after offset with radius $r_1 = r_0 + |\vec{a}|$ so that $A > r_1$ and the measurement sphere includes the minimum sphere, the amount of information from an information-theory perspective shall not be affected by the offset $\vec{a}$ even if the number of samples is not increased and the measurement is still performed considering a minimum sphere of radius r_0, corresponding to a measurement with the AUT centered in the measurement sphere.

To retrieve this information, a correction amounting to $C^{sm}_{hkl}(k|\vec{a}|)$ and $D^{l}_{mk}(\theta_a, \phi_a)$ must be applied to the new measurement $w'(A, \chi, \theta, \phi)$ if acquired with equiangular sampling and an amount of samples M corresponding to a measurement with a centered AUT and a minimum sphere of radius r_0. $w'(A, \chi, \theta, \phi)$ includes the displaced SWCs T'_{smn}. This allows $w(A, \chi, \theta, \phi)$ to be obtained instead. Upon application of FFT-based NFFFTs on the reconstructed $w(A, \chi, \theta, \phi)$, the SWCs of the AUT when centered in the measurement system, T_{hkl}, are retrieved. However, these terms are embedded in a summation with the unknown T_{hkl}, so that the application of a correction amounting to $C^{sm}_{hkl}(k|\vec{a}|)$ and $D^{l}_{mk}(\theta_a, \phi_a)$ is only analytically possible if T'_{smn} is known, which has a higher band-limit order B' and requires a larger amount of measurement samples for its calculation from $w'(A, \chi, \theta, \phi)$.

The suggested approach is the application of a multiplicative parallax [15] correction factor $h(r_i, \chi, \theta_i, \phi_i)$, calculated based on the estimation of the difference between $w'(A, \chi, \theta, \phi)$ and $w(A, \chi, \theta, \phi)$ stemming from the different relative measurement distance r_i from the center of the offset minimum sphere to the probe for each measurement point i. Additionally, the probe's boresight is not pointing towards the center of the offset minimum sphere for each point i, but with an offset (θ_i, ϕ_i), corresponding to the probe's view angle. In this paper, the approach used also introduces this difference in the correction factor. After applying the parallax correction, an estimation of $w(A, \chi, \theta, \phi)$, namely $\tilde{w}(A, \chi, \theta_{\text{plx}}, \phi_{\text{plx}})$, is obtained instead, so that:

$$\begin{aligned} h(r_i, \theta_i, \phi_i) w'(A, \chi, \theta, \phi) &= \tilde{w}(A, \chi, \theta_{\text{plx}}, \phi_{\text{plx}}) \approx \\ &\approx w(A, \chi, \theta, \phi). \end{aligned} \tag{8}$$

The angles $\theta_{\text{plx}}, \phi_{\text{plx}}$ describe a non-equiangular sampling on the minimum sphere, resulting from the projection of the equiangular sampling on the measurement sphere onto the displaced minimum sphere.

The irregular sampling grid prevents the usage of FFT-based NFFFTs. To enable them, an interpolation to an equiangular grid with the same number of samples is performed. Upon application of FFT-based NFFFTs on the interpolated $\tilde{w}(A, \chi, \theta, \phi)$, an estimation of the SWCs of the AUT when centered in the measurement system, $\widetilde{T_{hkl}} \approx T_{hkl}$, is retrieved.

In the following subsections, two approaches are followed:

- A classical, optical approach based on adjusting the Free Space Losses (FSPL) and the phase of each measured

point according to the relative measurement distance from the center of the minimum sphere with radius $r_i \neq A$ for each point i.
- A probe-only approach that automatically includes the effect of the difference between r_i and A by adding a compensation based on the difference of the probe pattern for each point in near field and the difference in the observation angle.

Both approaches require the projection of the measurement points of an equiangular sampling from the measurement sphere of radius $r = A$ onto the offset minimum sphere, with the corresponding calculation of the new distance r_i per measurement point i. This is done by converting the sampling points from spherical coordinates (θ, ϕ) to cartesian (x, y, z), applying the offset $\vec{a} = (x_0, y_0, z_0)$, and converting back to spherical, so that the translated coordinates $(r_i, \theta_{\text{plx}}, \phi_{\text{plx}})$ are defined as

$$\begin{aligned} r_i &= \sqrt{(x-x_0)^2 + (y-y_0)^2 + (z-z_0)^2} \\ \theta_{\text{plx}} &= \left| \cos^{-1}\left(\frac{z-z_0}{r_i}\right) \right| \\ \phi_{\text{plx}} &= \tan^{-1}\left(\frac{y-y_0}{x-x_0}\right) \end{aligned} \quad , \tag{9}$$

with (x, y, z) obtained from the classical coordinate transformation

$$\begin{aligned} x &= r_0 \sin(\theta)\cos(\phi) \\ y &= r_0 \sin(\theta)\sin(\phi) \\ z &= r_0 \cos(\theta) \end{aligned} \quad . \tag{10}$$

A. Optical Approach: FSPL and Phase Correction

The optical approach is known [1], [2] and will be included in the next IEEE Std. 1720 (2024) [15]. The correction factor does not depend on the view angle in this case, and it is given by $h_{\text{optical}}(r_i) = K(r_i)\mathrm{e}^{-jk\varphi(r_i)}$, with $K(r_i)$ being an amplitude offset, and $\varphi(r_i)$ being a phase offset. These are defined as:

- Amplitude offset $K(r_i)$: calculated as the difference of the FSPL for each measurement point i based on the relative distance r_i between them and the center of the offset minimum sphere, and compared with the FSPL for the case of a minimum sphere centered in the measurement sphere. Applying the Friis transmission equation, the offset is simplified to

$$K(r_i) = \left(\frac{r_0}{r_i}\right) \quad . \tag{11}$$

- Phase offset $\varphi(r_i)$: the $\varphi(r_i)$ term in the phase term $\mathrm{e}^{-jk\varphi(r_i)}$ depends only on the difference of distances, or equivalent radii, so that

$$\varphi(r_i) = (r_i - r_0) \quad . \tag{12}$$

Summarizing the multiplicative correction factor for the optical case is

$$h_{\text{optical}}(r_i) = \left(\frac{r_0}{r_i}\right) \mathrm{e}^{-jk(r_i - r_0)} \quad . \tag{13}$$

B. Probe Approach: SWE

This approach is based on analytically calculating the differences in the probe pattern in near field with help of the transmission formula, described by (1), for both the offset and the centered setups. This is done by applying the equation so that the right term is fully known, which allows to retrieve the left term, i.e., the "measurement" or, in this case, the probe pattern for given distances and angles [16].

Thereby, it is assumed that the term T_{smn} in Eq. (1) is the probe's SWCs in transmission mode, R^{tx}_{smn}, and that the probe response coefficients $P_{s\mu n}$ are calculated for the SWCs of a Hertzian dipole, i.e., as if the equivalent probe pattern would not affect the measurement. The equivalent view angle of the probe for each sampling point i is calculated as the difference between the angular position of the sampling points for equiangular sampling and the position of their projection onto the offset minimum sphere, namely

$$(\theta_i, \phi_i) = (\theta_{\text{plx}}, \phi_{\text{plx}}) - (\theta, \phi), \tag{14}$$

so that the correction factor becomes

$$\begin{aligned} &h_{\text{probe}}(r_i, \chi, \theta_i, \phi_i) = \\ &\quad = \sum_{\substack{smn \\ \mu}} R^{\text{tx}}_{smn} D^n_{\mu m}(\theta_i, \phi_i, \chi) P^{\text{dipole}}_{s\mu n}(kr_i) \end{aligned} \quad . \tag{15}$$

C. Uncertainty Sources

To enable the usage of FFT-based NFFFTs, an interpolation to the regular equiangular grid is performed after correction. However, four main uncertainty sources influence the result of the correction:

- The probe approach relies on a previous, perfect knowledge of the measuring probe. Any uncertainty in its characterization and its positioning and orientation directly influence results.
- The approach relies on a perfect knowledge of the offset $\vec{a} = (x_0, y_0, z_0)$.
- With respect to the AUT's minimum sphere, the sampling points are retrieved at $(\theta_{\text{plx}}, \phi_{\text{plx}})$. This grid will have an accumulation of measurement points (over-Nyquist) at positions for which $r_i < r_0$, while suffering from undersampling at positions for which $r_i > r_0$. This will affect the performance of the interpolation in the $r_i > r_0$ regions, especially with respect to maxima/minima occurring in them.
- Considering a real measurement with finite dynamic range and a real probe, measurement points acquired at certain (θ_i, ϕ_i) positions that may correspond with, or approach, probe pattern minima (nulls) will compromise the accuracy of the reconstruction.

IV. Validation

To validate the probe approach introduced in Subsection III-B, two sets of numerical experiments are carried out with known AUT SWCs, T_{smn}, and probe SWCs, $R_{\sigma\mu\nu}$. In the first

one, a measurement of the AUT is retrieved at a certain measurement distance A by using the Wacker formula described by Eq. (1). In the second one, the "offset" experiment, Eq. (7) is used with an offset $\vec{a} = (x_0, y_0, z_0)$ before using the Wacker formula described by Eq. (1) to generate a measurement of the offset AUT on an equiangular grid at a measurement distance A from the center of the measurement sphere. For both experiments, the equiangular grid at which the near-field measurement is generated is the same and it is calculated to fulfill the Nyquist criterion for the centered case, so that the offset measurement is, formally, undersampled.

A. Experiments

The workflow of the validation is:

- The AUT's NF is calculated at distance A and as measured by the given probe for both the centered and the offset case.
- The offset case is corrected using the probe-based approach explained in Subsection III-B, including interpolation.
- The AUT's NF for the centered case and for the corrected offset case are compared.
- Both NF patterns are used to retrieve the SWCs T_{smn} of the centered case and the estimation $\widetilde{T_{hkl}}$ of the offset case.
- Both sets of previously retrieve SWCs are used to calculate the AUT's FF, and both FF patterns are compared.

The experiments are carried out at $f = 6\,\text{GHz}$, using MVG'S QH400, an asymmetrical open boundary quad-ridge horn, as AUT [17]; and a standard symmetrical horn antenna as probe. The minimum sphere has a radius of approximately $r_0 = 0.4\,\text{m}$. The offset applied is $\vec{a} = (x_0, y_0, z_0) = (30\,\lambda, 30\,\lambda, 30\,\lambda) = (1.5\,\text{m}, 1.5\,\text{m}, 1.5\,\text{m})$, and the measurement distance A is chosen as double the equivalent minimum sphere after the offset, i.e., $A = 2r_1 = 2(r_0 + |\vec{a}|) \approx 3\,\text{m}$. The resolution used for the simulated acquisition is $\Delta\theta = \Delta\phi = 3°$.

Since the value of the cross-polar component is very low in horn antennas for the $\theta = 0°$ cut (it's a null), the $\theta = 45°$ cut is shown instead. Fig. 1 shows this cut, normalized, with the Co-Polar component in the upper subfigure and the Cross-Polar component in lower one. The offset pattern in FF is not included to avoid more clutter in the figure. Note that the resolution for FF and NF patterns is different: the NF patterns are shown with the measurement resolution of $\Delta\theta = \Delta\phi = 3°$, while the FF patterns have been reconstructed with a resolution of $\Delta\theta = \Delta\phi = 1°$. As described previously, the patterns after correction are not exactly equal to the reference patterns, i.e., the patterns for a centered measurement. However, it can be seen that the differences are negligible.

B. Practical Considerations

Operating and interpolating around the pole, the sphere's singularity, may result problematic and result in `NaN` results,

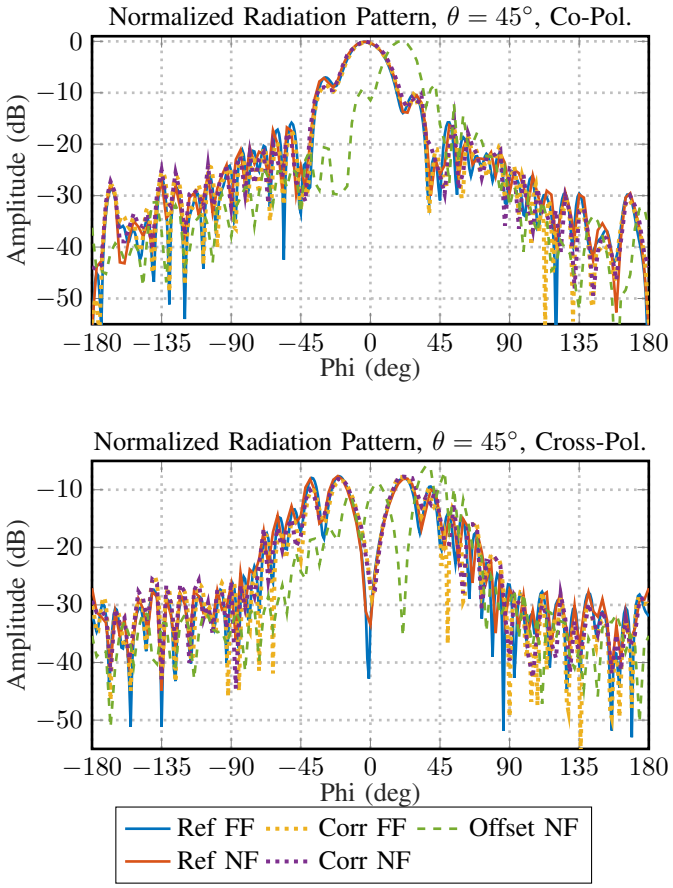

Fig. 1: Comparison between AUT-centered measurement and AUT-offset measurement after correction.

as well as in distorsion depending on the chosen field components. This is also true when applying the correction factor $h_{\text{probe}}(r_i, \chi, \theta_i, \phi_i)$, where it is easy to operate the wrong field components. It is recommended to apply the correction using Cartesian field components $\vec{E} = (E_x, E_y, Ez)$ to avoid the polarization rotation of $\vec{E} = (E_\theta, E_\phi)$ components around the pole. On the other hand, and while interpolating on Cartesian components is indeed possible, it is recommended to use $\vec{E} = (E_V, E_H)$ components to simplify the interpolation by one dimension. Additionally, depending on the chosen interpolation approach, a few `NaN` values may still occur. A further cut-wise 1-D interpolation is recommended to treat these cases.

V. Conclusion

An novel approach for the spherical near-field measurement of offset antennas, has been introduced. The approach allows to confidently measure offset antennas that cannot be centered, as often occurs in vehicular measurements, in their near field without increasing the number of samples. This approach relies on correcting the effects of different distance and the probe's view angle on each measurement point, so that the corrected data is an estimation of the near-field measurement

of a centered antenna.

The approach does not rely on an increase in the number of samples due to the enlargement of the minimum sphere due to the displacement of the AUT, and keeps the same number of samples required for a centered measurement. Additionally, the method allows to use FFT-based NFFFTs, thus avoiding the matrix (pseudo)inversions required by other offset-compensation methods and providing robustness. As seen by the results, the offset is successfully corrected and the uncertainties stemming from the taken assumptions are limited.

REFERENCES

[1] F. Saccardi, A. Scannavini, F. Mioc, L. J. Foged, and K. Zhao, "Over-the-air tests of 5G devices with direct measurements at reduced distance and parallax compensation," in *2021 Antenna Measurement Techniques Association Symposium (AMTA)*, 2021, pp. 1–5.

[2] F. Mioc, F. Saccardi, A. Scannavini, L. J. Foged, and K. Rutkowski, "Reduced distance OTA testing methodologies for automotive applications," in *2022 Antenna Measurement Techniques Association Symposium (AMTA)*, 2022, pp. 1–6.

[3] A. Scannavini, F. Mioc, K. Rutkowski, M. Mercier, F. Saccardi, and L. J. Foged, "Experimental validation of automotive OTA measurements at close distance," in *2022 16th European Conference on Antennas and Propagation (EuCAP)*, 2022, pp. 1–4.

[4] J. E. Hansen, *Spherical near-field antenna measurements*. IET, 1988, vol. 26.

[5] R. Cornelius, A. A. Bangun, and D. Heberling, "Investigation of different matrix solver for spherical near-field to far-field transformation," in *9th European Conference on Antennas and Propagation (EuCAP)*. IEEE, 2015, pp. 1–4.

[6] R. Cornelius, D. Heberling, N. Koep, A. Behboodi, and R. Mathar, "Compressed sensing applied to spherical near-field to far-field transformation," in *10th European Conference on Antennas and Propagation (EuCAP)*. IEEE, 2016, pp. 1–4.

[7] C. Culotta-López, *Fast Near-Field Measurements by Application of Compressed Sensing*. Dissertation, RWTH Aachen University, 2021.

[8] H. Nyquist, "Certain topics in telegraph transmission theory," *Transactions of the American Institute of Electrical Engineers*, vol. 47, no. 2, pp. 617–644, 1928.

[9] C. E. Shannon, "Communication in the presence of noise," *Proceedings of the IRE*, vol. 37, no. 1, pp. 10–21, 1949.

[10] O. Bucci, G. D'Elia, and M. Migliore, "A general and effective clutter filtering strategy in near-field antenna measurements," *Microwaves, Antennas and Propagation, IEE Proceedings -*, vol. 151, pp. 227 – 235, 07 2004.

[11] L. Foged, L. Scialacqua, F. Mioc, F. Saccardi, P. Iversen, L. Shmidov, R. Braun, J. Araque Quijano, and G. Vecchi, "Echo suppression by spatial-filtering techniques in advanced planar and spherical near-field antenna measurements [AMTA corner]," *Antennas and Propagation Magazine, IEEE*, vol. 55, pp. 235–242, 10 2013.

[12] G. Hindman and A. C. Newell, "Reflection suppression in large spherical near-field range," in *Antenna Measurement Techniques Association Symposium (AMTA)*, 2005, pp. 270–275.

[13] L. J. Foged, F. Saccardi, F. Mioc, and P. O. Iversen, "Spherical near field offset measurements using downsampled acquisition and advanced NF/FF transformation algorithm," in *2016 10th European Conference on Antennas and Propagation (EuCAP)*, 2016, pp. 1–3.

[14] F. Saccardi, L. J. Foged, F. Mioc, and P. O. Iversen, "Application of the translated-SWE algorithm to echo reduction of spherical near-field measurements with undersampling," in *2017 11th European Conference on Antennas and Propagation (EUCAP)*, 2017, pp. 2856–2860.

[15] "IEEE draft recommended practice for near-field antenna measurements," *IEEE Std 1720/D3-2024*, pp. 127–128, 2024.

[16] C. Culotta-López and D. Heberling, "Reduced sampling scheme for planar near-field measurements using pointwise probe correction in the spherical harmonics basis," in *Photonics and Electromagnetics Research Symposium (PIERS)*. IEEE, 2019, pp. 1–8.

[17] (2024, 8) Open boundary quad-ridge horns. Microwave Vision Group (MVG). [Online]. Available: https://www.mvg-world.com/media/2480/download/reference